ACS APPLIED POLYMER MATERIALS

Article

Cite This: ACS Appl. Polym. Mater. 2019, 1, 997−1005

pubs.acs.org/acsapm

Corona Treatment for Nanotransfer Molding Adhesion

Michael E. Deagen,[†,‡] Edwin P. Chan,[§] Linda S. Schadler,[†,‡] and Chaitanya K. Ullal*[,†,‡]

[†]Department of Materials Science and Engineering and [‡]Center for Lighting Enabled Systems and Applications, Rensselaer Polytechnic Institute, Troy, New York 12180, United States

[§]Materials Science and Engineering Division, National Institute of Standards and Technology, 100 Bureau Drive, Gaithersburg, Maryland 20899, United States

Supporting Information

ABSTRACT: Corona discharge treatment offers a facile, robust, and scalable technique for adhesion promotion in nanotransfer molding. In contrast to conventional plasma treatment, which requires vacuum operation, corona treatment at ambient pressure enabled patterning of woodpile structures of PDMS with smaller feature dimensions (70 nm line width) and across a wider range of treatment doses. Similarities and differences between plasma (batch) and corona (continuous) treatment were established using dyne testing to capture the effects of treatment on surface wettability of PDMS. Evaluating spatiotemporal evolution of wettability through dyne tests enabled a common axis for direct comparison of the two process configurations in terms of dose. Both treatment types formed surface films of oxidized PDMS, which were characterized through compressive buckling tests of the PDMS−oxide bilayer. Corona treatment, by forming a thinner oxide film, extended the range of treatment doses and feature sizes exhibiting successful pattern transfer. Reduction in adhesion at high treatment dose was attributed to a weak boundary layer at the bonded interface. Demolding was studied via peel tests and AFM analysis to reveal that both plasma and corona treatment etch the stamp material (PFPE), underscoring the benefits of low treatment dose for process throughput as well as stamp lifetime. While both treatments displayed comparable etch rates as a function of dose, microscopic bumps on corona-etched stamps indicate a higher surface temperature compared to plasma-etched stamps. By optimizing adhesion for nanotransfer molding with a surface treatment well-suited to continuous processing, corona treatment provides a practical and economical approach to layer-by-layer additive manufacturing at the nanoscale.

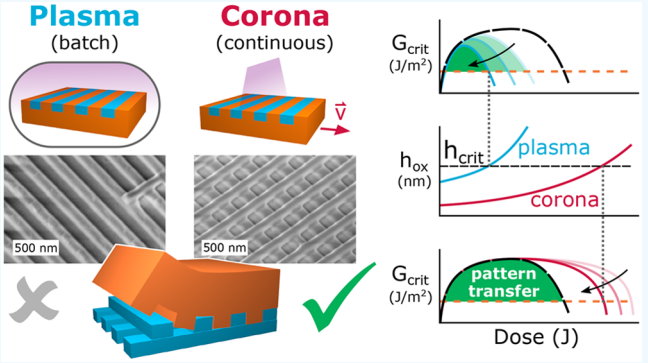

KEYWORDS: *stamping, soft lithography, plasma, woodpile, dyne testing*

INTRODUCTION

Borrowing concepts from early days of the printing industry, researchers have created well-defined nanoscale patterns at relatively low cost with a toolbox of techniques collectively known as soft lithography.[1] Transfer molding, one such technique, offers a three-dimensional approach to large-area micro- and nanofabrication. Using recessed features of an elastomeric mold (stamp) to define the pattern for each layer, transfer molding involves filling the indentations of the stamp with ink, curing the ink, transferring the pattern to a substrate, and repeating this process layer by layer.[2] Sufficient ink−substrate adhesion prevents unwanted separation, or delamination, of ink from the substrate as the stamp is peeled away. To achieve ink−substrate adhesion, previous approaches have employed partial curing,[2] an intermediate adhesive layer,[3] a liquid bridge to extract the ink upon evaporation,[4] or a sacrificial planarizing film later burned away.[5] While successful in some cases, these techniques rely on relatively weak intermolecular forces to bond adjacent layers.

Recently, transfer molding of poly(dimethylsiloxane) (PDMS) lines into woodpile structures using perfluoropolyether (PFPE) stamps has been achieved using plasma treatment for adhesion promotion.[6] In addition to forming polar surface groups that condense when brought together to form covalent interfacial linkages, exposure of PDMS to plasma treatment produces a silica-like oxide film at the surface.[7−9] Growth of the oxide film depends on plasma dose, defined as plasma generator power multiplied by duration of exposure.[10−12] It has been empirically shown that overexposure to plasma treatment eventually leads to a less robust interface, but the mechanism of adhesive failure is unclear.[13−16] During the peeling step of transfer molding, interfacial separation occurs at the weakest interface, ideally the stamp−ink (demolding) interface (Figure 1a). For plasma- or corona-bonded PDMS, a range of treatment levels can potentially provide sufficient

Received: January 14, 2019
Accepted: April 2, 2019
Published: April 2, 2019

DOI: 10.1021/acsapm.9b00028
ACS Appl. Polym. Mater. 2019, 1, 997−1005

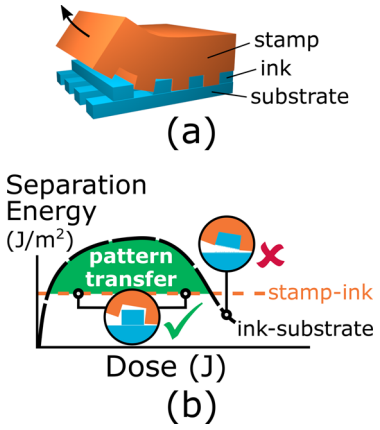

Figure 1. (a) Schematic representation of stamp peeling (demolding) during transfer molding. (b) Separation energy (quantitatively the critical energy release rate, G_{crit}) for interfaces of interest as a function of pretreatment dose. Energetic competition between stamp−ink and ink−substrate adhesion determines the preferred fracture path (and range of successful transfer molding). Black dashed curves show the expected increase and eventual decrease in adhesion for flat bonded PDMS.

ink−substrate bonding (Figure 1b). When applied to transfer molding of woodpile structures at the nanoscale, the oxide film leads to delamination even at relatively low plasma doses when the thickness of the oxide exceeds a critical value.[17] Therefore, the optimal conditions for adhesion consist of maximizing coverage of reactive surface groups while minimizing the thickness of the oxide film.

Corona treatment, or more specifically dielectric barrier discharge treatment, has seen significant commercial use as a surface pretreatment technique in the printing and coating industries that require functionalization of polymers with polar surface groups.[18−20] Unlike plasma treatment that is limited to batch processing due to vacuum requirements, corona treatment can be operated at ambient conditions, thus making it amenable to continuous, roll-to-roll (R2R) processing.[21,22] Although corona treatment offers a simple, economical alternative to plasma bonding of PDMS, the lack of quantitative power output on some systems limits the ability to quantify the level of treatment.[23] Additionally, corona and plasma treatments are often discussed jointly,[24−26] but different operating conditions render a side-by-side correlation elusive. In a continuous configuration, corona dose is calculated by dividing generator power by electrode width and substrate velocity.[27]

In this work, we demonstrate corona treatment as a low-cost, R2R-compatible surface treatment technique for layer-by-layer transfer molding at the nanoscale. We compared plasma and corona treatment in terms of dose using the critical surface tension, γ_c. We find that corona treatment enables the patterning of smaller line widths and successful transfer over a wider range of treatment dose. Stamp−ink and ink−substrate separation forces were quantified using peel tests. Etching of the stamp during plasma and corona treatment underscored the importance of brief treatment for extending stamp lifetime and increasing process throughput. Compressive buckling of the PDMS−oxide bilayer revealed a significantly thinner oxide film formed by corona treatment, avoiding the early onset of delamination observed for plasma treatment. Ultimately, corona treatment provides a facile route to multilayer patterning of smaller feature sizes with the added benefit of compatibility with continuous, R2R processing configurations.

METHODS

Materials. Silicon master patterns comprising 1-D periodic rectangular channels were purchased from LightSmyth Technologies (Eugene, OR) with pattern periods ranging from 140 nm to 6 μm (see Supporting Information Table S1). Perfluoropolyether (PFPE, Fluorolink MD-700) was purchased from Cornerstone Technology (Newark, DE) and combined with 1 mass% 2,2-dimethoxy-2-phenylacetophenone (DMPA) photoinitiator from Sigma-Aldrich. Low-viscosity, UV-curable divinylpoly(dimethylsiloxane) (DVPDMS) ink was prepared by combining vinyl-terminated PDMS (DMS-V21) with 5 mass % vinyl modulator (SIT7900.0) and 17 mass % (25−35% methylhydrosiloxane)−dimethylsiloxane copolymer (HMS-301) from Gelest. UV-h-PDMS was prepared following Schmid and Michel[28] and replacing the catalyst with Pt(II) acetylacetonate, which undergoes a UV-induced thermal-frontal hydrosilylation.[29] In both DVPDMS ink and UV-h-PDMS, Pt(II) acetylacetonate (Sigma-Aldrich) was used in a ratio of 500 ppm with respect to the number of vinyl groups. Sylgard 184 PDMS from Dow Corning was prepared in a 10:1 ratio (base:cross-linker) by mass. Dyne probe liquids of varying surface tension (33 mN/m−56 mN/m) were prepared by combining formamide (Promega) and 2-ethoxyethanol (Sigma-Aldrich) following ASTM D2578, with 1 mg/mL bromophenol blue (Sigma-Aldrich) for visual contrast (see Table S2).

Stamp and Peel Sample Preparation. Stamps were prepared by casting PFPE prepolymer against silicon master patterns and UV-curing in an N_2 atmosphere, followed by selective filling with DVPDMS ink.[6] Ink was cured inside the stamp prior to plasma or corona treatment by exposing to UV light (UV-A 6 W hand lamp, VWR) for 15 m prior to curing in an oven at 110 °C.

Peel test samples with 10 mm width were prepared using a multistep molding process (Figure S1). Patterned PDMS peel samples were prepared by spin-coating low-viscosity DVPDMS ink into the mold followed by a thin support layer of UV-h-PDMS (3000 rpm, 30 s), partially curing, and backfilling the mold with Sylgard 184 PDMS. The UV-h-PDMS support layer prevented pattern collapse of the smallest features (140 nm and 280 nm period), and the procedure was kept the same for the larger features (600 nm and 6 μm period) for consistency.

Plasma and Corona Treatment. Plasma treatment was performed in a 10 MHz inductively coupled plasma (ICP) chamber (PDC-32G) from Harrick Plasma (Ithaca, NY) at 107 Pa [800 mTorr] and 18 W power (Figure 2a). Corona treatment was performed with a 4.5 MHz hand-held corona treater (BD-20AC) from Electro-Technic Products (Chicago, IL) with the wire electrode attachment. The device was mounted above a roll-to-roll setup with controllable web speed (1 mm/s−50 mm/s), and the distance between sample and electrode was maintained at 5 mm (Figure 2b). An exhaust line behind the corona electrode provided an air flow that greatly improved uniformity of the corona discharge. Samples requiring a corona dose above the dose achievable at 1 mm/s web speed were sent through multiple passes (e.g., 3× and 6×). For both plasma and corona treatment, process gas was ambient air. Samples were bonded immediately (within 60 s) following treatment to avoid hydrophobic recovery of the PDMS surface. Water contact angle measurements (Figure S2) show the rapid increase in hydrophilicity of PDMS (Sylgard 184 and DVPDMS) as a function of treatment dose, followed by a gradual recovery of hydrophobicity over the course of 125 h. PFPE exhibits a slight decline in water contact angle upon exposure to surface treatment but overall remains hydrophobic ($\theta_{H_2O} > 70°$) even at high treatment dose.

Full Factorial Dyne Testing. In dyne testing, the critical surface tension of the substrate (γ_c) relative to the surface tension of the probe liquid (γ_{probe}) determines film formation. A uniform wetting film forms when $\gamma_c \geq \gamma_{probe}$, whereas the film breaks up into droplets when $\gamma_c < \gamma_{probe}$. PDMS samples for dyne testing were prepared by casting Sylgard 184 PDMS directly onto paper grids and curing at

DOI: 10.1021/acsapm.9b00028
ACS Appl. Polym. Mater. 2019, 1, 997−1005

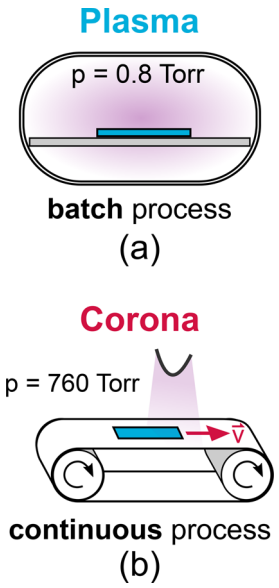

Figure 2. Schematic configurations of (a) plasma and (b) corona treatment as batch and continuous processes, respectively.

room temperature for at least 72 h. The grid enabled sample alignment with the corona electrode and definition of the scale for image analysis. Both Sylgard 184 and the DVPDMS ink used for nanotransfer molding contain PDMS with vinyl-curing groups and show a rapid reduction in water contact angle after treatment followed by hydrophobic recovery (Figure S2). For dyne testing experiments under corona treatment, PDMS samples were held stationary beneath the corona electrode. Immediately following plasma or corona treatment (within 60 s), probe liquid was dispensed from a transfer pipet onto a cleanroom cloth (TechniCloth, Texwipe) and dragged across the sample in one swift motion.

Full factorial experiments were run for both plasma and corona dyne tests, with six dyne probe liquids and five treatment durations for a total of 30 factor-level combinations in each experiment. A top-down optical image was recorded 3 s after the probe liquid was deposited. Plasma-treated PDMS samples showed wetting or nonwetting behavior uniformly across the entire sample for a given probe liquid, whereas corona-treated PDMS samples exhibited a wetted region of interest (ROI) surrounded by a nonwetting region further away from the electrode. Therefore, image analysis of corona-treated samples, using ImageJ, involved binarizing the image and extracting coordinates of the ROI. This analysis approach revealed the wettability gradient for a given treatment duration when plotted alongside ROIs from other probe liquids (Figure 3). Only one probe liquid was used per PDMS sample; therefore, the wettability gradients shown are a superposition of multiple samples.

Compressive Buckling of Oxidized PDMS. Samples of uniaxially prestrained Sylgard 184 PDMS ($\varepsilon_{pre} \approx 20\%$) in a clamp apparatus were subjected to plasma or corona treatment for a fixed treatment dose to form a bilayer comprising a stiff oxide film atop a soft PDMS substrate. Upon removal of the tensile strain, a periodic buckling pattern spontaneously formed on the oxide surface due to the strain mismatch between the stiff oxide film versus the softer PDMS supporting layer. The periodicity of the buckling pattern was averaged across three positions along each sample using AFM (Figure S7).

Peel Testing. Peel tests were performed in a T-Peel configuration on a TA-XT2i Texture Analyser (Stable Micro Systems, Surrey, United Kingdom) at a peel rate of 500 μm/s as described in earlier work.[17] At much higher peel rates, viscoelastic behavior of the stamp or substrate material would significantly increase the measured strain energy release rate, G_{crit}.[30] To quantify stamp demolding energy, DVPDMS lines were transferred from PFPE peel samples onto flat substrates of Sylgard 184 PDMS following plasma or corona

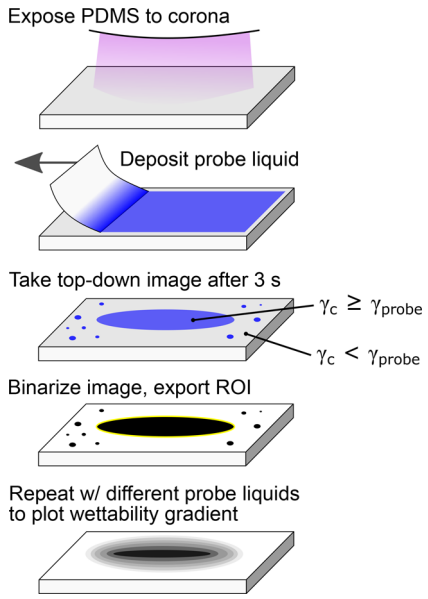

Figure 3. Procedure for visualizing gradient wettability of corona-treated PDMS using dyne testing. A series of probe liquids of varying surface tension reveal the lower limit of the critical surface tension, γ_c, of the PDMS surface as a function of location on the sample. In areas where γ_c is less than the surface tension of the probe liquid, γ_{probe}, the deposited liquid film spontaneously withdraws into isolated droplets within a few seconds. A full factorial experiment of several corona treatment durations, and γ_{probe} values provided the spatiotemporal evolution of γ_c as a function of treatment dose.

treatment (Figure 4a). Interlayer bond strength was simulated by bonding two orthogonally patterned PDMS peel samples (Figure 4b), in addition to flat Sylgard 184 PDMS samples.

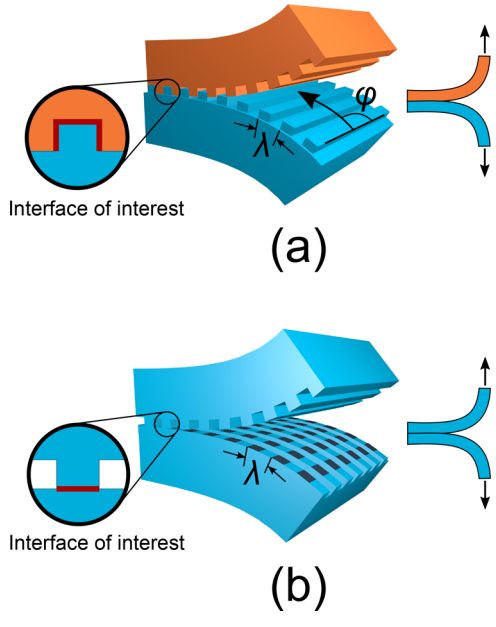

Figure 4. Illustration of peel samples for quantifying (a) demolding energy and (b) interlayer bond strength. Schematics on the right show the macro-scale configuration of the T-Peel test and insets below highlight the interface of interest in red. In the demolding experiments represented by (a), the angle between the patterned lines and the peeling direction, φ, was varied as 0 or 90° (φ = 90° shown). In (b), lines were bonded orthogonally to simulate a woodpile interface.

DOI: 10.1021/acsapm.9b00028
ACS Appl. Polym. Mater. 2019, 1, 997−1005

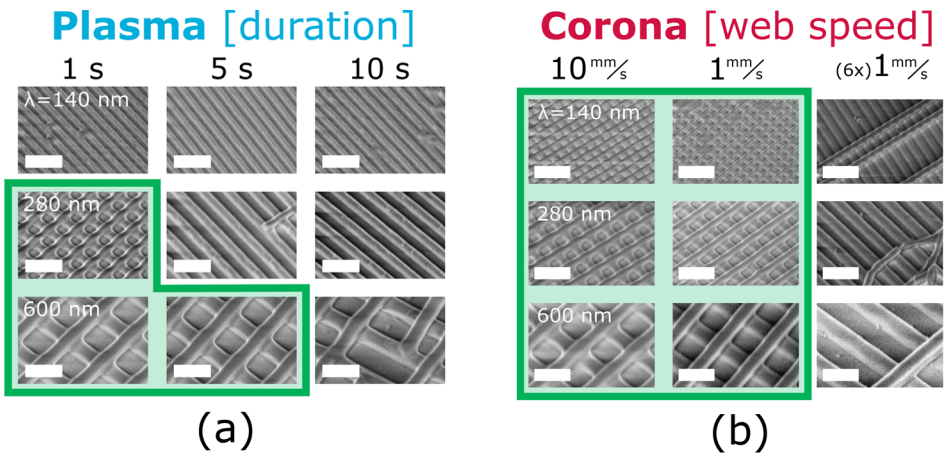

Figure 5. SEM images of two-layer woodpile transfer using (a) plasma treatment and (b) corona treatment, with successful transfer outlined in green. The treatment parameter (i.e., duration for plasma treatment, web speed for corona treatment) is shown atop each column. For corona treatment, longer exposures were achieved through multiple passes beneath the electrode indicated in parentheses. Feature period of each row is 140 nm, 280 nm, and 600 nm. Scale bars are 500 nm.

RESULTS

Success of Transfer from Plasma versus Corona Treatment. Earlier demonstrations of plasma treatment for nanotransfer molding adhesion only showed success with brief plasma exposure, requiring systematically lower plasma dose for smaller feature sizes and failing to achieve successful transfer for 70 nm wide (140 nm period) lines (Figure 5a).[17] Here, corona treatment not only achieved successful transfer of these 70 nm wide (140 nm period) lines, but successful transfer of all feature sizes occurred over at least an order of magnitude of exposure to corona (Figure 5b). Additionally, corona treatment on both the nano- and microscale lines showed a consistent cutoff between successful transfer versus delaminated lines (see Figure S3).

Estimating Corona Dose by Mapping Gradient Wettability Evolution. This new implementation of dyne testing, capable of mapping wettability gradients, enabled us to compare and contrast plasma (batch) and corona (continuous) treatment. Dyne tests following plasma treatment enabled mapping of γ_c as a function of plasma dose. γ_c, which represents the transition between nonwetting and wetting regions, was modeled as a sigmoidal evolution from a lower limit of 24 mN/m (γ_c of untreated PDMS[31,32]) to an upper limit of 72 mN/m (γ_c of silica[33]). An empirical fit to the dyne testing data from plasma treatment yielded

$$\gamma_c = 73 - 49e^{-(0.008\times D)^2} \quad (1)$$

where D represents the plasma dose, defined as generator power multiplied by duration of exposure. For plasma treatment, the dose affected wettability uniformly across the sample for a given treatment.

In corona treatment, the intensity of the corona on the sample varies depending on distance from the electrode.[34] Therefore, local corona dose, D, is a function of position, y, along the sample:

$$D(y) = P(y) \times t \quad (2)$$

where $P(y)$ is the corona power distribution along y and t is the duration of exposure.

We use a Cauchy–Lorentz distribution to model $P(y)$

$$P(y) = \frac{A}{\pi b\left[1 + \left(\frac{y}{b}\right)^2\right]} \quad (3)$$

and the spatial evolution of the critical surface tension as a function of dose was estimated by substituting eq 2 into eq 1. The A and b parameters in eq 3 describe the shape and magnitude of the Cauchy–Lorentz distribution, respectively (see Figures S4–S6). For a sample traveling at a fixed velocity beneath the corona electrode along the y-direction, such as in a R2R configuration, the corona dose is then

$$D = \frac{\int P(y)\,dy}{\vec{v}} = \frac{A}{\vec{v}} \quad (4)$$

where the integral of the Cauchy–Lorentz distribution is reduced to the fitting parameter A. By use of A = 700 and b = 0.8 for our configuration, wettability gradients from corona treatment showed good agreement across all treatments from 1 s to 30 s.

A Thinner Oxide Film from Corona Treatment. Compressive buckling, an established approach for analyzing the oxidized PDMS bilayer formed upon plasma treatment,[10−12,35] enabled comparison of relative oxide thickness formed through plasma or corona treatment as a function of dose. Because of a strain mismatch between the stiff oxide thin film and the soft PDMS supporting layer, a periodic buckling pattern forms with a period, d, that is directly proportional to thickness of the film, h_f:

$$d = 2\pi h_f\left(\frac{\bar{E}_f}{3\bar{E}_s}\right)^{1/3} \quad (5)$$

$\bar{E}_f$ and $\bar{E}_s$ are the plain strain moduli, $\bar{E} = E/(1-\nu^2)$, of the film and substrate, respectively.[11] To a first-order approximation, we assume that plasma oxidation process creates a discrete, stiff skin layer on the surface of the PDMS. While the amplitude of the buckling pattern depends on the level of prestrain, d is insensitive to strain (see Bayley et al.[11]). Based on the relative magnitude of d, h_f formed by corona treatment is ~25% of that formed by plasma treatment for an equivalent dose (Figure 6). The monotonic increase in d suggests h_f increases with plasma or corona treatment dose. While E_f may

DOI: 10.1021/acsapm.9b00028
ACS Appl. Polym. Mater. 2019, 1, 997−1005

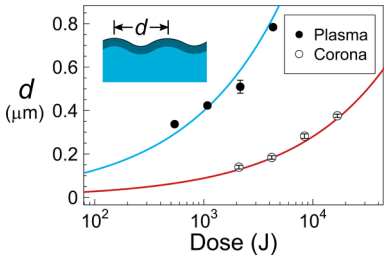

Figure 6. Characteristic period, d, of compressive buckling of the PDMS−oxide bilayer as a function of dose. Prestrained PDMS ($\varepsilon_{pre} \approx 20\%$) was exposed to varying levels of plasma/corona treatment, and the buckling pattern formed spontaneously upon removal from strain. Curves showing square root fits to the experimental data provide a guide to the eye. Error bars represent standard deviation of buckling period from three discrete regions of each sample.

vary between plasma and corona treatment, a large difference in film modulus ($E_f^{plasma}/E_f^{corona} \approx 64$) would be necessary to explain the observed difference in d through E_f alone. Below a dose of 2 kJ, corona-treated PDMS did not show buckling, indicating the prestrain value of $\varepsilon_{pre} \approx 20\%$ fell below the required critical strain, ε_c, to form the mechanical instability for such a thin film. Assuming E_f = 70 GPa, E_s = 1.6 MPa, ν_f = 0.17, and ν_s = 0.5 from earlier reported values for plasma-treated PDMS,[11] $h_f \cong 7$ nm for d = 1 μm. We assume to a first approximation that the oxidation process proceeds similarly on Sylgard 184 PDMS and the DVPDMS ink used for nanotransfer, both of which comprise PDMS with vinyl groups for cross-linking through hydrosilylation.

Demolding and Interlayer Separation Forces as a Function of Dose. Demolding and interlayer separation forces determine the probability of successful transfer of ink from the stamp onto a substrate. We use peel tests to quantify the stamp demolding energy, quantified by G_{crit}, as a function of pattern orientation and treatment dose. Figure 7a shows good correlation between G_{crit} and dose for both plasma and corona treated stamps. Here, the period of patterned lines was 600 nm. Demolding energy depended upon pattern orientation, and a consistently lower mean average peel force was required when the line direction was parallel to the direction of crack propagation (φ = 0) compared to the orthogonal case (φ = 90°). Both treatment types and pattern orientations showed an unexpected reduction in demolding force as a function of treatment dose.

To further understand the reduction in demolding energy as a function of dose, G_{crit} (for φ = 0 orientation) was quantified as a function of feature size for high and low corona dose. Large patterns (6 μm period) did not exhibit a pronounced reduction in G_{crit}, but a size-dependent reduction in G_{crit} for subμm patterns indicates that the reduction is caused by etching of the stamp surface during treatment (Figure 7b). Etching of stamp material as a function of plasma and corona dose was confirmed using AFM (see Figure S8).

G_{crit} of flat bonded PDMS samples was quantified as a function of plasma and corona treatment dose (Figure 8). Both treatments produced a rapid initial rise in bond strength compared to untreated control samples whose G_{crit} was below the resolution of the peel test apparatus. At an intermediate range of dose, interfacial cracks propagated into the bulk of some samples, causing cohesive failure (CF). An eventual drop-off in G_{crit} at high dose is consistent with earlier studies in the PDMS plasma-bonding literature.[13−15]

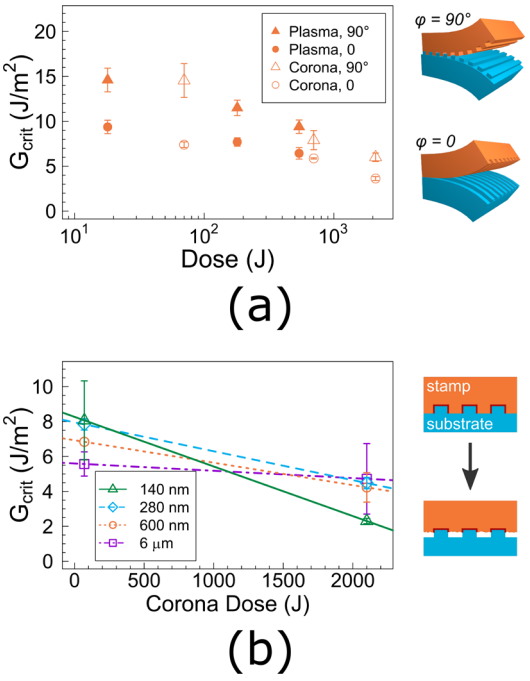

Figure 7. Measurement of demolding energy, G_{crit}, (a) for 600 nm period DVPDMS lines as a function of treatment type, pattern orientation, and treatment dose and (b) size-dependent reduction of G_{crit} as a function of feature size and corona treatment dose. Insets show (a) pattern orientation with respect to peel direction and (b) how etching of the stamp reduces the stamp−ink interfacial area. Trendlines connecting mean average peel force serve as a guide to the eye. Error bars represent standard deviation of mean average peel force across three replicates.

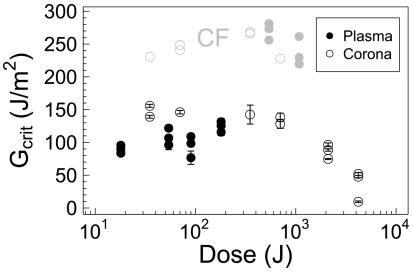

Figure 8. Adhesive strength of flat PDMS following varying plasma or corona dose. Error bars represent standard deviation of steady-state peel force for a given replicate. Three replicates were performed for each factor-level combination. Samples that failed through cohesive failure (CF) are shown as gray symbols.

Interlayer bond strength of DVPDMS lines of varying feature periods following plasma and corona treatment was measured using peel tests of orthogonally bonded lines (see Figure 4b) to simulate a woodpile interface. Some samples exhibited semicohesive failure (SCF), a macroscopically visible phenomenon where cracks were diverted from the DVPDMS interface of interest into the UV-h-PDMS support layer (see Figure S9). Broadly, plasma- and corona-treated PDMS displayed similar adhesive behavior as a function of dose, and patterned samples displayed lower G_{crit} than reference samples of flat Sylgard 184 PDMS.

PFPE Roughening during Corona Treatment. While plasma and corona treatment exhibit similar behavior in terms of stamp demolding energy and PDMS interfacial adhesion, a

DOI: 10.1021/acsapm.9b00028
ACS Appl. Polym. Mater. 2019, 1, 997−1005

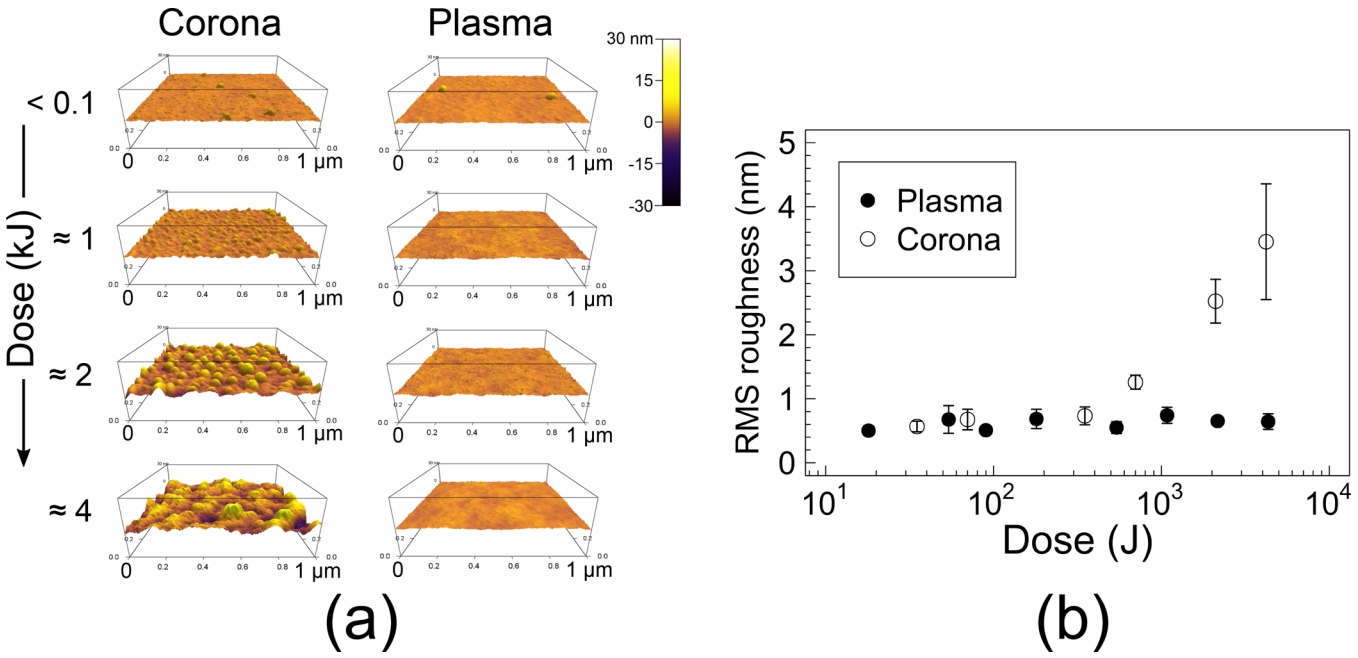

Figure 9. (a) AFM topography and (b) roughness of plasma- and corona-treated PFPE stamp as a function of dose. Error bars represent standard deviation of roughness measurements for a given sample.

pronounced difference in morphology of PFPE was observed as a function of plasma or corona dose. While both treatments etched PFPE, plasma treatment had little effect on topography of PFPE compared to corona treatment as measured using AFM (Figure 9a). Corona treatment led to formation of "bumps" along the surface with increasing dose and increased roughening of the surface is captured by RMS roughness (Figure 9b). Similar bumps have been observed in earlier studies of corona treatment on polypropylene and polyethylene.[22,36,37]

DISCUSSION

Improved Transfer from Corona Treatment. The success of transfer molding depends on the competition between the separation energy, G_{crit}, of the stamp−ink and ink−substrate interface (see Figure 1b). Ideally, successful pattern transfer would occur across a range of treatment doses. While plasma treatment revealed a feature size dependence on adhesion related to the thickness of the oxide film,[17] corona treatment demonstrated the ability to pattern all feature sizes across the full treatment range expected for PDMS. Corona treatment, as evidenced by compressive buckling experiments, forms a thinner oxide film as a function of dose than its plasma treatment counterpart. Therefore, corona treatment requires a much higher dose to produce a similar critical oxide thickness, h_{crit}, and achieves successful transfer at the nanoscale (70 nm line width) across a much larger process window compared with batch plasma treatment (Figure 10).

Reduced Adhesion at High Dose. Corona-bonded patterns displayed a transition from successful transfer to unwanted delamination above 2 kJ irrespective of feature size (Figure S3). This onset of delamination coincides with the expected drop in adhesion at high treatment dose,[13−16] suggesting a similar mechanism for the reduction in adhesion at high treatment doses. One potential mechanism, discussed by Owen and Smith in the context of hydrophobic recovery, involves condensation of silanol groups on the surface.[8,38] A high density of silanol groups may also lead to surface chain scission through backbiting reactions,[39] forming low-molecular-weight oxidized material (LMWOM). This LMWOM, which includes cyclic siloxane oligomers,[40] has been observed at the surface of PDMS subjected to a variety of treatments.[41,42]

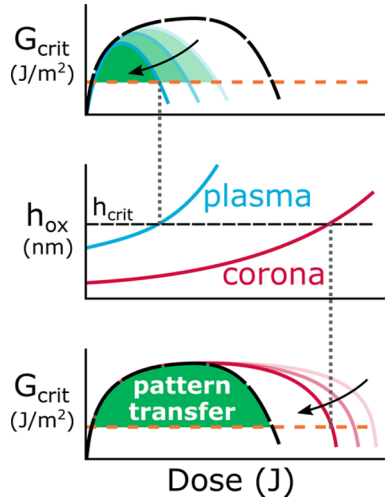

Figure 10. At submicrometer scales, depending upon the relative thickness of the plasma-oxidized film, h_{ox}, a feature size dependence on adhesion may be observed that reduces the range of treatments showing successful pattern transfer. Minimizing the relative thickness of this oxide film enables patterning of finer features and expands the window of successful treatments for pattern transfer.

At low dose, both plasma and corona treatments facilitate a rapid rise in adhesion as polar surface groups form. At high dose, LMWOM eventually forms a weak boundary layer. Provided that the oxide film does not exceed a critical thickness, the eventual reduction in adhesion is due to a weak boundary layer of LMWOM that forms. As a result, no size dependence on adhesion was observed for corona-bonded

DOI: 10.1021/acsapm.9b00028
ACS Appl. Polym. Mater. 2019, 1, 997−1005

PDMS lines, and the onset of delamination occurred at a dose (>2 kJ) consistent with the reduction in adhesion of flat PDMS.

Applicability of Full Factorial Dyne Testing Technique. Dyne testing, through the full factorial approach presented here, served as a rapid, facile technique to measure wettability gradients induced by nonuniform surface treatments. Dyne testing measures critical surface tension, γ_c, rather than surface energy, γ_{sv}, of a solid, but it has been shown that γ_c and γ_{sv} are symbatic.[43] The method is not universally suited for analyzing effects on dissimilar materials. As a result, comparison of plasma and corona treatment was performed using the same material (PDMS) and series of dyne probe liquids.

The Cauchy−Lorentz distribution we use to estimate the power distribution beneath the corona electrode has a physical basis. During dielectric barrier discharge, a series of microarcs, or streamers, randomly emanate from the corona electrode.[44] The Cauchy−Lorentz distribution represents the probability that a line rotated about an axis at a height b above a line intersects the line at any given point. Given the good agreement with spatiotemporal dyne testing data, the assumption of a uniform distribution of angles appears to hold well in this case, where separation between sample and electrode was relatively small. At larger separation distances, ionic drift would need to be taken into account and the angular distribution would be expected to follow the empirically derived Warburg distribution where corona current density depends on $\cos^5 \theta$.[45,46]

The dose parameter for batch plasma treatment is defined as the product of plasma generator power (W) and treatment duration (s).[10−12] To define the effect of treatment on the surface of a sample, a unit area is needed to give surface power density (e.g., W/m^2). This unit area depends on the equipment used. On the other hand, for continuous corona treatment, the dose (e.g., J/m^2) is calculated by dividing generator power by web speed and electrode width.[27] Comparing batch plasma treatment and continuous corona treatment remains difficult, as generator power efficiency or other system parameters may affect the ability to directly compare the techniques. Full factorial dyne testing is impartial to the system configuration, establishing an equivalence solely based on the physical effects of surface treatment on wettability. Therefore, the unit area assumed when quantitatively discussing plasma and corona dose in this work has an implicit but unknown unit area corresponding to the plasma instrument described in the Methods section.

Distinctions between Plasma and Corona Treatment. Plasma and corona surface treatments inherently differ in their operating pressure and plasma type, resulting in differences related to surface modification. For example, while both plasma and corona treatments form polar hydroxyl and silanol groups on the surface of PDMS, corona treatment has also been shown to form a small number of nitrogen functionalities.[26,47] We observed similarities in terms of demolding energy and etch rate and stark differences in PFPE morphology and oxide growth kinetics.

Surface temperature during corona treatment may significantly exceed the temperature during plasma treatment.[47] In our work, this difference is evidenced by the bump morphology of PFPE as a result of increased corona dose. Comparing to the time−temperature dependence of bump formation on corona-treated polyethylene,[37] a similar evolution in morphology occurs by either increasing temperature or treatment time. There, bump formation was hypothesized as surface migration of LMWOM. Further evidence for the bumps comprising LMWOM has been shown in polypropylene, where the bumps are removed upon rinsing.[22,48] While etch rate appears comparable for plasma and corona treatments, we attribute microscale morphological differences of PFPE to an increased surface temperature.

A significant reduction in oxide film thickness from corona treatment highlights the dependence of growth kinetics on treatment conditions. Nania et al. studied oxidation of PDMS as a function of dose for air plasma treatment and modeled the reaction as a frontal vitrification that depends upon pressure of operation, potentially due to a reduction in mean free path of ions.[12] Within a range of pressures for air plasma treatment (50 Pa−150 Pa), the data were found to collapse when plotted as dose normalized by pressure, D/P. Our results, which extend across 3 decades of pressure (10^2 Pa−10^5 Pa), further support their hypothesis that growth rate slows at higher pressures. However, we find better agreement when normalizing by $D/\sqrt{P}$ rather than D/P (Figure S10). While the mean free path is expected to scale inversely with pressure, another quantity (e.g., diffusion length and average ion momentum) that scales inversely with square root of pressure may elicit further insights into plasma oxidation. More study is needed to reveal the nature of oxide film growth as a function of treatment conditions and plasma type.

Effect of Treatment on Demolding Energy and Stamp Lifetime. We find that demolding energy exhibits anisotropic behavior for one-dimensional periodic lines, where demolding energy is higher when the direction of crack propagation is perpendicular to the direction of the lines (φ = 90°). These results are consistent with demolding measurements by Landis et al. in the context of nanoimprint lithography (NIL),[49] where edges encountered by the crack during interfacial separation may act as pinning points for crack propagation.

A fluorinated stamp material was useful in preventing unwanted adhesion between stamp and substrate following plasma treatment. However, both plasma and corona treatment displayed evidence of etching the stamp material. The extent of etching was negligible for replication of relatively large features but becomes significant when defining nanoscale features. While stamps were not reused in this study, etching would diminish reusability of stamps by altering the height of patterned features as well as conditions for residual-layer-free filling of the stamp.[6] Alteration of the surface energy of the PFPE from surface treatment could also affect subsequent coating processes; however, supporting contact angle measurements (Figure S2a) show that the impact on surface energy is diminutive compared to etching. This result emphasizes the benefit of using the lowest plasma or corona dose possible, not only for extending reusability of the stamp but also for maximizing throughput in the case of R2R corona treatment where a lower dose corresponds to a higher web speed.

CONCLUSIONS

Corona treatment was employed to facilitate interlayer adhesion for transfer molding of nanoscale PDMS lines, enabling transfer of smaller patterns (70 nm line width) across a wider range of exposures compared to plasma treatment. An equivalence between plasma (batch) and corona (continuous) treatments was established in terms of dose by quantifying

DOI: 10.1021/acsapm.9b00028
ACS Appl. Polym. Mater. 2019, 1, 997−1005

spatiotemporal wettability with dyne testing. Increased plasma and corona dose led to a reduction in demolding energy, and etching of the PFPE stamp material led to this size-dependent reduction by reducing stamp-ink contact area. Differences between the two treatments in terms of pressure and surface temperature are highlighted by the oxide growth kinetics and the PFPE morphology, respectively. By minimizing growth of the oxide film, corona treatment provides robust adhesion for transfer molding adhesion at the nanoscale while simultaneously offering a configuration compatible with continuous, roll-to-roll manufacturing processes.

■ ASSOCIATED CONTENT

Supporting Information

The Supporting Information is available free of charge on the ACS Publications website at DOI: 10.1021/acsapm.9b00028.

Silicon master pattern dimensions, dyne probe liquid formulations, description of peel sample preparation, SEMs of corona-bonded PDMS lines, derivation of dose equivalence using dyne test data, AFMs of compressively buckled PDMS−oxide bilayers, AFMs of plasma- and corona-etched stamps, patterned PDMS peel sample data, and oxide growth normalized by pressure (PDF)

■ AUTHOR INFORMATION

Corresponding Author

*E-mail: ullalc@rpi.edu.

ORCID

Michael E. Deagen: 0000-0002-8034-0667
Edwin P. Chan: 0000-0003-4832-6299
Chaitanya K. Ullal: 0000-0002-7178-897X

Notes

The authors declare no competing financial interest.

■ ACKNOWLEDGMENTS

This article is based on work supported by the National Science Foundation under cooperative agreement EEC-0812056, the Graduate Research Fellowship Program under Grant DGE-1247271, and New York State under NYSTAR Contract C090145. Any opinion, findings, and conclusions or recommendations expressed in this article are those of the author(s) and do not necessarily reflect the views of the National Science Foundation. Certain instruments and materials are identified in this paper to adequately specify the experimental details. Such identification does not imply recommendation by the National Institute of Standards and Technology; nor does it imply that the materials are necessarily the best available for the purpose. This work is a contribution of NIST, an agency of the U.S. Government, and not subject to U.S. copyright. The authors also thank Christopher M. Stafford for helpful conversations.

■ REFERENCES

(1) Xia, Y.; Whitesides, G. M. Soft Lithography. *Angew. Chem., Int. Ed.* **1998**, *37*, 550−575.

(2) Zhao, X. M.; Xia, Y. N.; Whitesides, G. M. Fabrication of Three-Dimensional Micro-Structures: Microtransfer Molding. *Adv. Mater.* **1996**, *8*, 837−840.

(3) Lee, J. H.; Kim, C. H.; Ho, K. M.; Constant, K. Two-Polymer Microtransfer Molding for Highly Layered Microstructures. *Adv. Mater.* **2005**, *17*, 2481−2485.

(4) Hwang, J. K.; Cho, S.; Dang, J. M.; Kwak, E. B.; Song, K.; Moon, J.; Sung, M. M. Direct Nanoprinting by Liquid-Bridge-Mediated Nanotransfer Moulding. *Nat. Nanotechnol.* **2010**, *5*, 742−748.

(5) Kothari, R.; Beaulieu, M. R.; Hendricks, N. R.; Li, S. K.; Watkins, J. J. Direct Patterning of Robust One-Dimensional, Two-Dimensional, and Three-Dimensional Crystalline Metal Oxide Nanostructures Using Imprint Lithography and Nanoparticle Dispersion Inks. *Chem. Mater.* **2017**, *29*, 3908−3918.

(6) Deagen, M. E.; Schadler, L. S.; Ullal, C. K. Wetting Regimes for Residual-Layer-Free Transfer Molding at Micro- and Nanoscales. *ACS Appl. Mater. Interfaces* **2017**, *9*, 36385−36391.

(7) Chaudhury, M. K.; Whitesides, G. M. Direct Measurement of Interfacial Interactions between Semispherical Lenses and Flat Sheets of Poly(Dimethylsiloxane) and Their Chemical Derivatives. *Langmuir* **1991**, *7*, 1013−1025.

(8) Owen, M. J.; Smith, P. J. Plasma Treatment of Polydimethylsiloxane. *J. Adhes. Sci. Technol.* **1994**, *8*, 1063−1075.

(9) Duffy, D. C.; McDonald, J. C.; Schueller, O. J.; Whitesides, G. M. Rapid Prototyping of Microfluidic Systems in Poly(Dimethylsiloxane). *Anal. Chem.* **1998**, *70*, 4974−4984.

(10) Chiche, A.; Stafford, C. M.; Cabral, J. T. Complex Micropatterning of Periodic Structures on Elastomeric Surfaces. *Soft Matter* **2008**, *4*, 2360−2364.

(11) Bayley, F. A.; Liao, J. L.; Stavrinou, P. N.; Chiche, A.; Cabral, J. T. Wavefront Kinetics of Plasma Oxidation of Polydimethylsiloxane: Limits for Sub-μm Wrinkling. *Soft Matter* **2014**, *10*, 1155−1166.

(12) Nania, M.; Matar, O. K.; Cabral, J. T. Frontal Vitrification of PDMS Using Air Plasma and Consequences for Surface Wrinkling. *Soft Matter* **2015**, *11*, 3067−3075.

(13) Jo, B.-H.; Van Lerberghe, L. M.; Motsegood, K. M.; Beebe, D. J. Three-Dimensional Micro-Channel Fabrication in Polydimethylsiloxane (PDMS) Elastomer. *J. Microelectromech. Syst.* **2000**, *9*, 76−81.

(14) Bhattacharya, S.; Datta, A.; Berg, J. M.; Gangopadhyay, S. Studies on Surface Wettability of Poly(Dimethyl) Siloxane (PDMS) and Glass under Oxygen-Plasma Treatment and Correlation with Bond Strength. *J. Microelectromech. Syst.* **2005**, *14*, 590−597.

(15) Befahy, S.; Lipnik, P.; Pardoen, T.; Nascimento, C.; Patris, B.; Bertrand, P.; Yunus, S. Thickness and Elastic Modulus of Plasma Treated PDMS Silica-Like Surface Layer. *Langmuir* **2010**, *26*, 3372−3375.

(16) Chen, C.; Wharton, K. Characterization and Failure Mode Analyses of Air Plasma Oxidized PDMS−PDMS Bonding by Peel Testing. *RSC Adv.* **2017**, *7*, 1286−1289.

(17) Deagen, M. E.; Chan, E. P.; Schadler, L. S.; Ullal, C. K. Size Effects in Plasma-Enhanced Nano-Transfer Adhesion. *Soft Matter* **2018**, *14*, 9220−9226.

(18) Owens, D. Mechanism of Corona−Induced Self-Adhesion of Polyethylene Film. *J. Appl. Polym. Sci.* **1975**, *19*, 265−271.

(19) Goldman, M.; Goldman, A.; Sigmond, R. The Corona Discharge, Its Properties and Specific Uses. *Pure Appl. Chem.* **1985**, *57*, 1353−1362.

(20) Gerenser, L.; Elman, J.; Mason, M.; Pochan, J. Esca Studies of Corona-Discharge-Treated Polyethylene Surfaces by Use of Gas-Phase Derivatization. *Polymer* **1985**, *26*, 1162−1166.

(21) Grace, J. M.; Gerenser, L. J. Plasma Treatment of Polymers. *J. Dispersion Sci. Technol.* **2003**, *24*, 305−341.

(22) Guimond, S.; Wertheimer, M. R. Surface Degradation and Hydrophobic Recovery of Polyolefins Treated by Air Corona and Nitrogen Atmospheric Pressure Glow Discharge. *J. Appl. Polym. Sci.* **2004**, *94*, 1291−1303.

(23) Haubert, K.; Drier, T.; Beebe, D. PDMS Bonding by Means of a Portable, Low-Cost Corona System. *Lab Chip* **2006**, *6*, 1548−1549.

(24) Strobel, M.; Walzak, M. J.; Hill, J. M.; Lin, A.; Karbashewski, E.; Lyons, C. S. A Comparison of Gas-Phase Methods of Modifying Polymer Surfaces. *J. Adhes. Sci. Technol.* **1995**, *9*, 365−383.

(25) Kruse, A.; Krüger, G.; Baalmann, A.; Hennemann, O.-D. Surface Pretreatment of Plastics for Adhesive Bonding. *J. Adhes. Sci. Technol.* **1995**, *9*, 1611−1621.

(26) Tóth, A.; Bertóti, I.; Blazsó, M.; Bánhegyi, G.; Bognar, A.; Szaplonczay, P. Oxidative Damage and Recovery of Silicone Rubber Surfaces. I. X-Ray Photoelectron Spectroscopic Study. *J. Appl. Polym. Sci.* **1994**, *52*, 1293−1307.
(27) Lindner, M.; Rodler, N.; Jesdinszki, M.; Schmid, M.; Sängerlaub, S. Surface Energy of Corona Treated PP, PE and PET Films, Its Alteration as Function of Storage Time and the Effect of Various Corona Dosages on Their Bond Strength after Lamination. *J. Appl. Polym. Sci.* **2018**, *135*, 45842.
(28) Schmidt, I.; Binder, K. Model Calculations for Wetting Transitions in Polymer Mixtures. *J. Phys. (Paris)* **1985**, *46*, 1631−1644.
(29) Sangermano, M.; Marchi, S.; Ligorio, D.; Meier, P.; Kornmann, X. UV-Induced Frontal Polymerization of a Pt-Catalyzed Hydrosilation Reaction. *Macromol. Chem. Phys.* **2013**, *214*, 943−947.
(30) Meitl, M. A.; Zhu, Z.-T.; Kumar, V.; Lee, K. J.; Feng, X.; Huang, Y. Y.; Adesida, I.; Nuzzo, R. G.; Rogers, J. A. Transfer Printing by Kinetic Control of Adhesion to an Elastomeric Stamp. *Nat. Mater.* **2006**, *5*, 33−38.
(31) Lee, L.-H. Enhancement of Surface Wettability of Abhesive Silicone Rubber by Oxidation. *J. Adhes.* **1972**, *4*, 39−49.
(32) Crocker, G. J. Elastomers and Their Adhesion. *Rubber Chem. Technol.* **1969**, *42*, 30−70.
(33) Olsen, D. A.; Osteraas, A. J. The Critical Surface Tension of Glass. *J. Phys. Chem.* **1964**, *68*, 2730−2732.
(34) Eifert, A.; Petit, J.; Baier, T.; Bonaccurso, E.; Hardt, S. Inscribing Wettability Gradients onto Polymer Substrates with Different Stiffness Using Corona Discharge in Point-to-Plane Geometry. *Appl. Surf. Sci.* **2015**, *330*, 104−110.
(35) Bowden, N.; Huck, W. T.; Paul, K. E.; Whitesides, G. M. The Controlled Formation of Ordered, Sinusoidal Structures by Plasma Oxidation of an Elastomeric Polymer. *Appl. Phys. Lett.* **1999**, *75*, 2557−2559.
(36) Blais, P.; Carlsson, D.; Wiles, D. Effects of Corona Treatment on Composite Formation. Adhesion between Incompatible Polymers. *J. Appl. Polym. Sci.* **1971**, *15*, 129−143.
(37) Kim, C.; Goring, D. Surface Morphology of Polyethylene after Treatment in a Corona Discharge. *J. Appl. Polym. Sci.* **1971**, *15*, 1357−1364.
(38) Lee, C.-L.; Homan, G. R. In *Silicone Elastomer Protective Coatings for High Voltage Insulators*; Conference on Electrical Insulation & Dielectric Phenomena, Annual Report 1981; IEEE: 1981; pp 435−443.
(39) Hillborg, H.; Gedde, U. Hydrophobicity Changes in Silicone Rubbers. *IEEE Trans. Dielectr. Electr. Insul.* **1999**, *6*, 703−717.
(40) Hillborg, H.; Karlsson, S.; Gedde, U. W. Characterisation of Low Molar Mass Siloxanes Extracted from Crosslinked Polydimethylsiloxanes Exposed to Corona Discharges. *Polymer* **2001**, *42*, 8883−8889.
(41) Kim, J.; Chaudhury, M. K.; Owen, M. J. Hydrophobic Recovery of Polydimethylsiloxane Elastomer Exposed to Partial Electrical Discharge. *J. Colloid Interface Sci.* **2000**, *226*, 231−236.
(42) Hillborg, H.; Ankner, J.; Gedde, U. W.; Smith, G.; Yasuda, H.; Wikström, K. Crosslinked Polydimethylsiloxane Exposed to Oxygen Plasma Studied by Neutron Reflectometry and Other Surface Specific Techniques. *Polymer* **2000**, *41*, 6851−6863.
(43) Owens, D. K.; Wendt, R. Estimation of the Surface Free Energy of Polymers. *J. Appl. Polym. Sci.* **1969**, *13*, 1741−1747.
(44) Schutze, A.; Jeong, J. Y.; Babayan, S. E.; Park, J.; Selwyn, G. S.; Hicks, R. F. The Atmospheric-Pressure Plasma Jet: A Review and Comparison to Other Plasma Sources. *IEEE Trans. Plasma Sci.* **1998**, *26*, 1685−1694.
(45) Warburg, E. Ueber die Spitzenentladung. *Ann. Phys.* **1899**, *303*, 69−83.
(46) Warburg, E. Characteristik des Spitzenstromes. *Handb. Phys.* **1927**, *14*, 154−155.
(47) Hollahan, J. R.; Carlson, G. L. Hydroxylation of Polymethylsiloxane Surfaces by Oxidizing Plasmas. *J. Appl. Polym. Sci.* **1970**, *14*, 2499−2508.
(48) Strobel, M.; Dunatov, C.; Strobel, J. M.; Lyons, C. S.; Perron, S. J.; Morgen, M. C. Low-Molecular-Weight Materials on Corona-Treated Polypropylene. *J. Adhes. Sci. Technol.* **1989**, *3*, 321−335.
(49) Landis, S.; Chaix, N.; Gourgon, C.; Leveder, T. Quantitative Characterizations of a Nanopatterned Bonded Wafer: Force Determination for Nanoimprint Lithography Stamp Removal. *Nanotechnology* **2008**, *19*, 125305.

DOI: 10.1021/acsapm.9b00028
ACS Appl. Polym. Mater. 2019, 1, 997−1005